Classification: PHYSICAL SCIENCES, Earth, Atmospheric, and Planetary Sciences

Title: Limited oxygen production in the Mesoarchean ocean

Frantz Ossa Ossa[1,2]*, Axel Hofmann[2], Jorge E. Spangenberg[3], Simon W. Poulton[4], Eva E. Stüeken[5], Ronny Schoenberg[1], Benjamin Eickmann[1,2], Martin Wille[6], Mike Butler[7], Andrey Bekker[8,2]

[1] *Department of Geosciences, University of Tuebingen, 72074 Tuebingen, Germany.*

[2]*Department of Geology, University of Johannesburg, 2092 Johannesburg, South Africa.*

[3]*Institute of Earth Surface Dynamics (IDYST), University of Lausanne, 1015 Lausanne, Switzerland.*

[4]*School of Earth and Environment, University of Leeds, Leeds LS2 9JT, UK.*

[5]*School of Earth & Environmental Sciences, University of St. Andrews, St. Andrews, KY16 9AL, UK.*

[6]*Institute of Geological Sciences, University of Bern, 3012 Bern, Switzerland.*

[7]*Environmental Isotope Laboratory, IThemba LABS, 2050 Johannesburg, South Africa.*

[8]*Department of Earth Sciences, University of California, Riverside, CA 9252, USA.*

*Correspondence to: frantz.ossaossa@gmail.com

Author contributions: F.OO., A.H., R.S. and A.B. designed research; F.OO., A.H. and A.B. performed research; F.OO., A.H., J.E.S., E.E.S., S.W.P., M.B. and A.B. acquired and analyzed data; F.OO. wrote the paper with significant input from all authors.

Abstract: The Archean Eon was a time of predominantly anoxic Earth surface conditions, where anaerobic processes controlled bio-essential element cycles. In contrast to oxygen oases well documented for the Neoarchean (2.8-2.5 billion years ago; Ga), the magnitude, spatial extent, and underlying causes of possible Mesoarchean (3.2-2.8 Ga) surface ocean oxygenation remain controversial. Here, we report $\delta^{15}N$ and $\delta^{13}C$ values coupled with local seawater redox data for Mesoarchean shales of the Mozaan Group (Pongola Supergroup, South Africa), which were deposited during an episode of enhanced Mn (oxyhydr)oxide precipitation between ~2.95 and 2.85 Ga. Iron and Mn redox systematics are consistent with an oxygen oasis in the Mesoarchean anoxic ocean, but $\delta^{15}N$ data indicate a Mo-based diazotrophic biosphere with no compelling evidence for a significant aerobic nitrogen cycle. We propose that in contrast to the Neoarchean, dissolved O_2 levels were either too low or too limited in extent to develop a large and stable nitrate reservoir in the Mesoarchean ocean. Since biological N_2 fixation was evidently active in this environment, the growth and proliferation of O_2-producing organisms were likely suppressed by nutrients other than nitrogen (e.g., phosphorus), which would have limited the expansion of oxygenated conditions during the Mesoarchean.

Keywords: oxygen oasis; nitrogen isotopes; nutrient limitation; oxygenic photosynthesis; Mesoarchean

Significance Statement: Episodic development of "oxygen oases" during the Archean Eon characterizes the hundreds of millions of years transition to permanent oxygenation in the atmosphere-hydrosphere system at the Great Oxidation Event (~2.4-2.3 Ga). One of these well-characterized "oxygen oases" is recorded in Mesoarchean (~2.95-2.85 Ga) sediments of the Pongola Supergroup. We show that in contrast to the Neoarchean (2.8-2.5 Ga), biological oxygen production in a shallow ocean having Mo-based nitrogen fixation was not sufficient to result in a dissolved nitrogen reservoir that would carry the isotopic effects of an aerobic nitrogen cycle. Nevertheless, it appears that low concentrations of bioavailable phosphorus, rather than nitrogen, suppressed the growth and expansion of oxygenic photosynthesizers, and may explain why pervasive and permanent oxygenation was delayed during the Archean Eon.

\body

A dramatic rise in atmospheric oxygen level during the Great Oxidation Event (GOE) at ~2.4 Ga is marked by the disappearance of mass-independent fractionation of sulfur isotopes, oxidation of detrital pyrite and uraninite, and the appearance of red beds, reflecting the irreversible transition from an anoxic to an oxic world (1-2). While it is widely accepted that oxygenic photosynthesis was a first-order control on the GOE (3), Archean shallow-marine "oxygen oases" and "whiffs" of atmospheric oxygen (O_2) have been proposed to have occurred up to several hundred million years prior to the GOE (4-18). However, while processes that drove oxygen production during transient and localized oxygenation events in the Neoarchean (2.8-2.5 Ga) are supported by a wide range of geochemical proxies (*e.g.*, 4-6, 13-18), those from the Mesoarchean (3.2-2.8 Ga) are constrained by only a limited number of studies (7-12).

The nitrogen (N) cycle from the early Archean up to ~2.7 Ga is widely considered to have been dominated by bioavailable ammonia (NH_4^+) under anoxic water column conditions (15, 16). Oxidation of NH_4^+ would have been suppressed in an early Archean ocean characterized by extremely low O_2 concentrations (15-17). Free O_2 is produced through oxygenic photosynthesis, the rate of which is mainly controlled by the concentrations of bioavailable N and phosphorus (P) (19-24). While the sedimentary $\delta^{15}N$ record suggests that N was bioavailable and that diazotrophic Mo-based nitrogenase dominated N_2 fixation in the Mesoarchean, the record also places a robust minimum age for the occurrence of aerobic N cycling at ~2.72 Ga in the Neoarchean (*e.g.*, 15, 16 and references therein). Indeed, prominent N isotope excursions in the Neoarchean provide evidence for temporary NH_4^+ oxidation, and thus the $\delta^{15}N$ record has been used to infer the development of locally oxygenated surface ocean environments after ~2.7 Ga (5, 15, 17, 18, 25).

Independently, stable isotope systematics of redox-sensitive elements such as Fe, Mo, U and S, as well as locally enhanced Mn (oxyhydr)oxide precipitation, support an earlier emergence of oxygenic photosynthesis and episodic development of "oxygen oases" in the Mesoarchean surface ocean (7-9, 11), well before currently accepted evidence for oxidative nitrogen cycling. Furthermore, phylogenomic estimates based on molecular clocks also suggest that cyanobacterial stems capable of oxygenic photosynthesis might find their roots in the Archean, with a development and progressive diversification starting as early as ~3.5 Ga (26-28). However, the factors that caused a delay in pervasive oxygenation of the atmosphere-hydrosphere system after the establishment of oxygenic photosynthesis in the early Archean remain poorly constrained, particularly with regard to the role of their two main bio-limiting nutrients, N and P (19-23). Modelling studies have demonstrated that low dissolved P concentrations would severely suppress the rate of oxygenic photosynthesis and ultimately the spatial extent of Archean oxygen oases (29). However, there is currently no consensus on dissolved P concentrations in the Archean ocean (21-23, 30-32).

In order to assess controls on the spatial development and intensity of Earth's first oxygen oases, we measured nitrogen ($\delta^{15}N$) and organic carbon ($\delta^{13}C_{org}$) isotopes, local water column redox proxies (Fe speciation and Mn concentrations), and elemental data for shales of the ~2.95-2.85 Ga Mozaan Group, Pongola Supergroup, South Africa (see Supplementary Information for geologic setting and all data). Our aim is to clarify the factors that controlled the nature and development of oxygen oases in the Mesoarchean.

Results and discussion

Water column redox reconstruction. Our samples span a shallow-marine (above wave base) depositional setting in the White Mfolozi Inlier, to a deeper-water (below wave base) equivalent in the Nongoma area, and comprise three sequences deposited at different water depths (Figs. 1, S1, S2; Table S1). In the White Mfolozi Inlier, sequence I, deposited in the most proximal, intertidal to shallow subtidal setting, is characterized by high Mn contents and Mn/Fe ratios compared to average values for shales of the Pongola Supergroup (33; Table S1), mostly high ratios of highly-reactive Fe to total Fe (FeHR/FeT) and high Fe/Al ratios (see Methods for detailed analytical techniques). Sequence II was deposited in a deep subtidal, but above fair-weather wave base setting, and shows a progressive decrease in Mn, Mn/Fe, FeHR/FeT and Fe/Al, while Mn and Fe contents are higher than in average Pongola shales (33; Table S1). The uppermost sequence III represents deepening to between fair-weather and storm wave base, and is characterized by persistently low Mn, Mn/Fe, FeHR/FeT and Fe/Al, with Mn and Fe contents similar to those in average Pongola shales (33; Table S1). In the more distal, deeper-water setting of the Nongoma area, where distinct compositional trends were not observed, Fe/Al ratios tend to be high, but Mn contents remain low and Mn/Fe ratios shift to values lower than the average for shales of the Pongola Supergroup (33; Table S1).

To explain these data, we invoke upwelling of anoxic waters that were rich in Fe^{2+} and Mn^{2+} into oxic shallow waters. Precipitation of Fe as (oxyhydr)oxide minerals may have started under low oxygen or anoxic conditions, potentially via photoferrotrophy in shallower waters directly overlying deeper anoxic waters (34), and this likely explains the observed Fe enrichments in the distal Nongoma setting (Fig. 1b). Fe(II) oxidation would have been progressive during upwelling, leading to increased FeHR/FeT and Fe/Al enrichments (Fig. 1a) as water depth shallowed through a redoxcline (as captured by sequence II in the White Mfolozi Inlier) into the shallow and locally oxygenated waters of sequence I, where Mn(IV) (oxyhydr)oxides precipitated (Fig. 1a; Fig 2). Increased Mn/Fe ratios in shallower waters thus reflect progressive removal of dissolved Fe(II) and/or enhanced precipitation of Mn (oxyhydr)oxides as upwelling anoxic waters reached the redox threshold for Mn(II) oxidation. However, sequence III in the White Mfolozi Inlier has Mn/Fe ratios similar to the average value for shales of the Pongola Supergroup, with no evidence for FeHR enrichment, likely reflecting deeper anoxic waters where there was limited oxidant availability to promote Fe- or Mn-

(oxyhydr)oxide precipitation in the water column. At first glance, Fe enrichments in shallower waters and their absence in deeper waters of the White Mfolozi Inlier may appear contradictory, since Fe enrichments are commonly taken to denote water column anoxia (35). However, our data are entirely consistent with current understanding of how Fe enrichment may be enhanced under anoxic ferruginous conditions, whereby one prominent pathway for developing high FeHR/FeT and Fe/Al ratios is via upwelling of deep, anoxic waters into shallower oxic settings (35, 36).

Once Mn and Fe (oxyhydr)oxides had formed and became deposited, they were then largely converted to carbonate minerals through microbial respiration during early diagenesis, as indicated by high Fe_{carb} concentrations in sediments of sequence I and II (Table S1). In support of this, highly negative $\delta^{13}C$ (between –22 and –13‰, VPDB) and $\delta^{18}O$ values (between –21 and –8‰, VPDB) indicate carbonate precipitation through organic carbon remineralization during diagenesis (7, 37). This happened below the sediment-water interface in sediments deposited below a water column characterized by relatively high rates of organic carbon (OC) burial (high productivity) (7). In contrast, Fe_{carb} is scarce in the deeper water sequence III and the more distal Nongoma setting (Table S1), where instead most of the Fe is associated with chlorite and stilpnomelane (7). It is thus likely that Fe (oxyhydr)oxides were converted to Fe-rich clay minerals during diagenesis in this setting, probably via reverse weathering (38). Another possibility involves conversion of Fe (oxyhydr)oxides into mixed ferrous/ferric phases such as green rust during settling (39, 40), before their final transformation to stilpnomelane and chlorite during diagenesis and metamorphism. Thermodynamic estimates based on the chemical composition of Fe-chlorite showed that Fe- and Mn-rich clay minerals of the Mozaan Group formed during diagenesis and metamorphism (37). Regardless of the precise nature of precursor Fe minerals, Fe/Al ratios much higher than those in average Pongola shales (33; Table S1) indicate that their precipitation gave rise to significant Fe enrichments in the deep-water sediments, and during upwelling of deep ferruginous waters into shallower oxic settings.

The $\delta^{13}C_{org}$ values average –27.6‰ in the shallow-water sequence I samples, reflecting isotopic fractionations expected during autotrophic CO_2 fixation (41). During deposition of sequence II, $\delta^{13}C_{org}$ values progressively decrease to the average value of –30‰, and down to –38‰ in the deep-water settings of the White Mfolozi Inlier and Nogoma areas (Fig. 1). The highly negative $\delta^{13}C_{org}$ values in these deeper-water, ferruginous settings likely reflect biological carbon cycling with a significant contribution from methanogens and methanotrophs (42). The variability in biological processes with water-depth might be linked to the water column redox

gradient, where (*1*) high Mn/Fe ratios and Mn(II) oxidation (which requires free O_2) are consistent with photoautotrophic CO_2 fixation and oxygenic photosynthesis in the shallow-water settings, and (*2*) Fe enrichments without Mn(II) oxidation (Mn/Fe ratios lower than the average Pongola shale values) are consistent with methanotrophs utilizing dissolved O_2 or Fe(III) compounds to oxidize methane at the redoxcline or chemocline, respectively, under hypoxic or anoxic conditions in deeper-water settings. In view of this, the water column appears to have been both redox and ecologically stratified.

N isotope systematics and preservation of primary isotopic signals. Our geochemical data suggest a shallow-water oxygen oasis in the Mesoarchean Pongola sea at ~2.9 Ga. If these conditions were stable and extensive enough to support oxic nitrogen metabolism, then this should be reflected in nitrogen isotope systematics, as observed in younger Neoarchean sedimentary successions (5, 15, 17, 18, 25). Large N isotope heterogeneity revealed by the NanoSIMS technique in isolated microfossils from the ~3.0 Ga Farrel Quartzite (Western Australia) has been linked to biological aerobic nitrification (43), indicating the emergence of this metabolic pathway even before deposition of the Mozaan Group. In ancient marine sediments, $\delta^{15}N$ values between –4 and +2‰ (Air-N_2) are usually attributed to isotopic fractionation imparted during biological N_2 fixation using the Mo-nitrogenase enzyme (Nif; 5, 15-18, 25). The use of V- (Vnf) and Fe-based (Anf) alternative nitrogenase enzymes produces more depleted $\delta^{15}N$ values, between –6 and –8‰ (15, 44). $\delta^{15}N$ values above +4‰ would provide compelling evidence for an aerobic N cycle coupling nitrification and denitrification/anammox processes (*e.g.*, 5, 15, 17, 18, 25). Nitrogen isotope values for 18 out of 22 samples fall in the range of –5 to +3‰ (Air-N_2), and reflect isotopic fractionation driven by Mo-based diazotrophy (Fig. 1; Table S2). Positive values above +4‰ are limited to 4 samples, including 2 from the White Mfolozi Inlier and 2 others from the more distal Nongoma area.

Here, we exclude abiotic sources for bioavailable nitrogen, because they were probably too small in magnitude and should have otherwise dominated the early Precambrian $\delta^{15}N$ record, counter to what is observed (15). However, several mechanisms can alter the original $\delta^{15}N$ values of marine biomass, ranging from early diagenesis to the thermal degradation of organic matter (OM) during deeper burial diagenesis and metamorphism (15, 45-48). The redox state of the water column, sedimentation rate, and OM accumulation can also impart different N

isotope fractionations between sinking organic particles and surficial marine sediments. NH_4^+ release during OM remineralization below the sediment-water interface and partial oxidation in pore waters can increase bulk sediment $\delta^{15}N$ ($\delta^{15}N_{bulk}$) values by ~4‰ under oxic diagenetic conditions, while this effect tends to be minimal during anoxic diagenesis, with an isotopic fractionation <1‰ (15, 45). The predominance of Fe- and Mn-carbonate minerals derived from the reduction of Fe- and Mn-(oxyhydr)oxides indicate anoxic diagenetic conditions (7, 37) and thus likely a minimal effect of early diagenetic processes on primary $\delta^{15}N$ values. Importantly, oxic diagenesis would result in isotopic compositions that reflect an aerobic nitrogen cycle, which is not seen in our dataset.

Organic-bound NH_4^+ can also be released through thermal devolatization of organic matter during burial diagenesis and metamorphism, resulting in a maximum increase in $\delta^{15}N_{bulk}$ values of 1–2‰ at greenschist facies, 3–4‰ at lower amphibolite facies, and up to 6–12‰ at upper amphibolite facies; even larger offsets can occur in sedimentary rocks affected by circulating fluids (46). The Mozaan Group experienced lower greenschist facies metamorphism (37), suggesting a maximum increase in $\delta^{15}N_{bulk}$ values of less than 2‰. In order to alleviate potential effects caused by mechanisms described above on $\delta^{15}N$ values, N isotope data were also measured on extracted kerogen ($\delta^{15}N_{ker}$) to compare with bulk sample data ($\delta^{15}N_{bulk}$). The offset between $\delta^{15}N_{bulk}$ and $\delta^{15}N_{ker}$ values allows evaluation of the extent of preservation of the N isotope signature imparted by the initially deposited biomass. Two samples from the Nongoma area showing evidence for hydrothermal processes are characterized by large offsets between $\delta^{15}N_{bulk}$ and $\delta^{15}N_{ker}$ values and very positive N isotope values (Fig. 1; Table S2), which likely supports post-depositional alteration by circulating fluids. Therefore, these 2 samples will not be further considered in this study. In contrast, the minimal offset in most of the studied samples supports good preservation of the primary isotopic signature (Fig. 1; Table S2). The samples with minimal offset between $\delta^{15}N_{bulk}$ and $\delta^{15}N_{ker}$ values also lack evidence of secondary alteration by later circulating fluids or hydrothermal processes (37). Furthermore, a minimal effect of post-depositional processes on the isotope composition of biomass is also indicated by the absence of co-variation among $\delta^{15}N$ and TN, $\delta^{15}N$ and C/N, $\delta^{15}N$ and $\delta^{13}C$, as well as between $\delta^{13}C_{TOC}$ and TOC for bulk sediments (Fig. 3). A weak negative co-variation between $\Delta^{15}N_{ker–bulk}$ (the difference between $\delta^{15}N_{ker}$ and $\delta^{15}N_{bulk}$) and total K further supports a minimal contribution of ammoniated phyllosilicates (*e.g.*, NH_4^+ substituted for K^+) with a distinct isotopic composition (see Fig. S4).

A lack of evidence for aerobic nitrogen cycling in the Mesoarchean Pongola basin oxygen oasis. In the modern ocean, where the main processes intrinsic to the aerobic N cycle, including N_2 fixation, nitrification, and denitrification/anammox, are at play, $\delta^{15}N$ values of +5 to +7‰ in sedimentary organic matter reflect ^{14}N loss to the atmosphere through denitrification and anammox in oxygen-minimum zones (48). Buried biomass is an indirect archive of this process, because organisms assimilate the isotopically heavy nitrate as a nutrient. Therefore, $\delta^{15}N$ values ≥ +4‰ found in Neoarchean marine sediments are interpreted to reflect temporary aerobic N cycling (*e.g.*, 5, 15, 17, 18, 25). In contrast, the nitrogen isotope data of the Mozaan Group are inconsistent with the establishment of a significant aerobic nitrogen cycle. Assuming that Mn(II) oxidation occurs at higher redox potential than NH_4^+ oxidation, redox conditions may have been sufficient for evolved nitrifying bacteria in the Pongola basin, because high Mn concentrations in sequence I indicate the precipitation of Mn(IV) oxyhydroxide minerals (7), which required O_2. Photochemical oxidation of Mn is inhibited under Fe-saturated conditions (49) and, unlike Fe(II), significant oxidation of Mn requires oxygen and a catalyst (50). It is thus likely that free O_2 was locally available in the water column during deposition of sequence I (7) and that the subtle increase in $\delta^{15}N_{ker}$ values (up to +5.2‰) measured in 2 samples from the upper part of sequence I (deposited at the redoxcline) may reflect nitrification/denitrification and uptake of residual nitrate in the water column (Figs. 2). However, the absence of a more compelling isotopic shift in $\delta^{15}N$ values over the extended stratigraphic interval indicates that NO_3^- (*i.e.* the residual nitrogen species that carries the isotopic information in the modern ocean) did not build up to high enough concentrations to be an important nitrogen source to the biosphere.

While the iron and manganese proxies have the capacity to promptly respond to redox perturbations on a local scale, the nitrogen isotope proxy requires the build-up of a dissolved nitrogen reservoir that carries the isotopic effects of redox reactions at the ecosystem scale. A good modern analog illustrating such a discrepancy between Mn (higher redox potential) and N (lower redox potential) cycles can be found in the Black Sea. Here, rapid oxygen-dependent microbial Mn(II) oxidation is observed at low micromolar (< 3-5 μM) dissolved oxygen contents in the suboxic zone of the Black Sea (51), where nitrification produces a maximum nitrate concentration of only 3.5 μM (52). However, this maximum nitrate level appears to be too low to leave an isotopic signature of aerobic N cycling (53) (in contrast to open ocean nitrate concentrations of up to ~35 μM, which leave an average $\delta^{15}N$ signal of around +5‰; ref 15 and references therein). Estimates of O_2 content based on $\delta^{56}Fe$ variations in

Mesoarchean oxygen oases suggest a maximum concentration of 10 μM (7, 11). Such dissolved O_2 levels are thus consistent with the potential activity of both Mn(II) oxidizing and nitrifying bacteria during deposition of the Mozaan Group.

It appears that the geographical extent of oxygen oases was likely too restricted in the Mesoarchean ocean to develop a nitrate reservoir that was large enough to leave an isotopic signature, which contrasts with their Neoarchean equivalents (assuming water-column O_2 concentrations were similar in the Mesoarchean and Neoarchean oxygen oases; 7, 11, 29). Overwhelming supply of reducing inputs (e.g., Fe(II) and Mn(II)) from submarine volcanism to the Mesoarchean ocean could have suppressed more widespread oxygenation and thus limited nitrification. However, iron formation (IF) secular records (e.g., 54, 55) indicate that volumetrically, the Neoarchean IFs are much larger than their Mesoarchean analogs, and yet the Neoarchean to early Paleoproterozoic IFs are characterized by compelling evidence for aerobic N cycling (5, 25, 56). It therefore appears that the reducing sinks from submarine volcanism were not the main driving factor that suppressed the expression of aerobic N cycle in the Mesoarchean ocean.

Implications for oxygenic photosynthesis in the Mesoarchean ocean. Overall, our data reveal an ecosystem that was dominated by Mo-based diazotrophy, in an oxygen oasis where a combination of the restricted spatial extent and low dissolved O_2 concentration likely limited the build-up of a sufficient nitrate reservoir to impart an isotopic expression of aerobic N cycling. In the modern ocean, cyanobacteria are the main N_2 fixers (57), and our data suggest that this relationship may extend back to the Mesoarchean. Mo-based diazotrophy requires soluble MoO_4^{2-} availability in the ocean. In the modern ocean, Mo is mainly delivered via riverine inputs following oxidative continental weathering, with a minor contribution from submarine hydrothermal systems (see ref. 16 and references therein). The mild Mo enrichment (relative to average concentration for the upper crust) recorded by the Mozaan Group (Table S1) suggests that dissolved Mo was available in this oxygen oasis (8). However, it has been shown that a very low Mo content (down to 1 nM, which is ca. 1% of modern seawater concentrations) can sustain Mo-based diazothrophy in modern environments (58). In view of this, submarine hydrothermal Mo inputs could have been sufficient to sustain Mo-based N_2 fixation in the Archean ocean (see ref. 16 and references therein). Moreover, it has also been demonstrated that continental Mo could have been mobilized and delivered to the ocean even

under Archean anoxic atmospheric conditions (O_2 concentration < 10^{-5} PAL; 59, 60 and references therein).

Free O_2 produced by oxygenic photosynthesis had an impact on the water-column redox and ecological gradients of the Pongola basin, as observed in stable isotope data confirming aerobic Fe and Mn cycling in shallow-water settings (7). Bioavailable N and P are the main nutrients that control marine productivity over time (*e.g.*, 19-23). Their scarcity may have limited biological O_2 production, resulting in delayed pervasive and permanent oxygenation of the atmosphere-hydrosphere system after the emergence of oxygenic photosynthesis in the Mesoarchean. Since our $\delta^{15}N$ data indicate that N was bioavailable in the Mesoarchean marine oasis, P scarcity could have been the main limiting factor in biological O_2 production, consistent with previous biogeochemical modelling (29). Indeed, we observe very low P contents in the Pongola sediments (Fig. 1; Table S1), which would be entirely consistent with the suggestion of widespread P limitation under global ferruginous conditions (21), prior to more extensive anoxic P recycling linked to the build-up of seawater sulfate following more expansive environmental oxygenation (22).

It is possible that positive $\delta^{15}N$ values in the ca. 3.2 Ga riverine deposits of the Moodies Group, South Africa, interpreted as evidence for denitrification (12), and a weakly oxidizing U cycle in the Mesoarchean ocean (11, 61), may reflect episodes of mild, local oxidizing conditions in the atmosphere-hydrosphere system (ref. 13 and references therein). However, estimates based on preserved Mesoarchean detrital uraninite in the Witwatersrand Supergroup (South Africa) deposited contemporaneous with the Pongola Supergroup suggest that atmospheric O_2 concentrations were lower than 3.2×10^{-5} atm (62). Furthermore, the general absence of $\delta^{15}N$ values above +4‰ in most Mesoarchean marine and continental deposits around the world (15, 16, 63; this study), is consistent with the view that low rates of biological O_2 production limited the geographical extent of oases and, ultimately, controlled the size of the seawater nitrate reservoir, which did not reach the level necessary to leave a more widespread and persistent isotopic signature of an aerobic N cycle. Regardless of the mechanism/s that controlled dissolved P concentrations in Archean oceans, oxygenation of Earth's early biosphere was apparently limited by a low supply of bio-available P, rather than N, under anoxic to very low-oxygen surface conditions.

Methods

Major and trace elements. Powdered samples were analysed for major element concentrations by X-ray fluorescence spectroscopy. Analysis was carried out on fusion beads, using a PANalytical MagiX Pro PW2540 spectrometer at the University of Johannesburg. Accuracy was checked with certified reference materials and was better than 1%. Elemental concentrations are reported in wt.% with a detection limit of 0.04 wt.%. Trace elements were measured at the Isotope Geochemistry Lab, University of Tuebingen (Germany) according to the analytical procedure previously described (10, 64). Around 30 mg of ashed powdered samples (heated to 600°C for 12 hours to ash organic compounds) were dissolved using a mix of concentrated and distilled HF (2 mL) and HNO_3 (0.3 mL) in screw-top 15 mL Savillex© PFA beakers at 120°C for 4 days. After evaporation at 80°C, samples were taken up in 1.5 mL 6 M HCl and re-dissolved in closed beakers at 130°C for 1 day. The samples were evaporated to incipient dryness at 90°C and reacted twice with 0.3 mL aliquots of concentrated HNO_3 with evaporation at 90°C in between to remove excess F and Cl. An aliquot of 5 M HNO_3 (1 mL) was added to the sample residues and heated at 80°C for ~1 hour for dissolving the samples. Analyses were performed in the iCap-Qc ICP-MS coupled to an ESI SC-2 DX auto-sampler with an ESI Fast uptake system equipped with a 4 mL sample loop. For analysis, solution samples in 1 mL 5 M HNO_3 were diluted twice; first in MQ water (dilution factor 1000) and second in an internal standard solution made of 0.3 M HNO_3 (dilution factor 10,000) containing a spike mixture of ^{6}Li (~3 ppb), In (~1 ppb), Re (~1 ppb), and Bi (~1 ppb). Analytical accuracy, estimated from the 1 r.s.d. of the mean, varied between 3 and 15% and was monitored by repeated measurements of reference materials OU-6, QS-1, W-2a, and AGV-2. Enrichment factors were calculated as $(element/Al)_{sample}/(element/Al)_{reference}$ using the average concentrations for the upper crust as reference (65).

Iron speciation analysis. Iron speciation analysis was performed at the University of Leeds, UK using a calibrated sequential extraction protocol followed by Fe analysis via AAS (66). This method is designed to quantify four different pools of Fe considered to be highly-reactive (FeHR) towards H_2S in surface and near-surface environments: (*1*) pyrite S extracted via Cr-reduction followed by trapping as Ag_2S, with Fe calculated assuming an FeS_2 stoichiometry (Fe_{Py}); (*2*) carbonate-associated iron extracted with a sodium acetate solution (Fe_{Carb}); (*3*) ferric oxides extracted with a dithionite solution (Fe_{Ox}); and (*4*) mixed-valence iron oxides, principally magnetite, extracted using ammonium oxalate (Fe_{Mag}). The total Fe content in ancient marine shales (FeT) represents the sum of FeHR and Fe bound in silicates (66, 67). It has been established that marine shales deposited under oxic water column conditions are

characterized by low ratios of FeHR/FeT < 0.22 driven by the lack of Fe mineral precipitation following transport of Fe(II) under anoxic water column conditions. Under anoxic water column conditions, FeHR/FeT ratios tend to be higher (above 0.38), whereas values between 0.22 and 0.38 are considered equivocal due to additional processes (*e.g.*, rapid sedimentation) that may obscure Fe enrichments under anoxic water column conditions (35). Furthermore, for anoxic water column conditions with FeHR/FeT > 0.38, FePy/FeHR < 0.7 represents ferruginous conditions, whereas FePy/FeHR values above 0.7−0.8 characterize euxinic conditions (35, 67). In some cases, FeHR can be converted to poorly reactive silicates (FePRS) during diagenesis resulting in apparently low FeHR/FeT ratios, which can be wrongly interpreted to reflect oxic water column conditions (35, 67). Therefore, it is required to pair FeT/Al ratios and FePRS concentrations in order to distinguish samples deposited under oxic from those deposited under anoxic water column conditions, where $FeT/Al \leq 0.55 \pm 0.11$ would indicate oxic water column conditions (67). FeT/Al > 0.66 would reflect local Fe enrichments either under anoxic water column conditions, or due to input of anoxic hydrothermal fluids into oxic seawater (67).

Carbon and nitrogen isotope analyses. The nitrogen isotope composition of bulk rock ($\delta^{15}N_{bulk}$) and the carbon and nitrogen isotope compositions of the extracted kerogen ($\delta^{13}C_{org}$, $\delta^{15}N_{ker}$) were determined by elemental analysis/isotope ratio mass spectrometry (EA/IRMS) at the Institute of Earth Surface Dynamics of the University of Lausanne (Switzerland), using a Carlo Erba 1108 (Fisons Instruments, Milan, Italy) elemental analyzer connected to a Delta V Plus isotope ratio mass spectrometer via a ConFlo III open split interface (both of Thermo Fisher Scientific, Bremen, Germany) operated under continuous helium flow (68, 69). The kerogen, the fraction of organic matter insoluble in organic solvents, non-oxidizing acids and bases, dispersed in lithified sediments, was isolated through several steps. These steps are based on the dichloromethane-extraction procedure followed by HF–HCl treatment at the Institute of Earth Surface Dynamics, University of Lausanne. The procedure modified from Durand and Nicaise (70) involved Soxhlet extraction with a mixture of methanol and dichloromethane for removal of the soluble organic fraction (bitumen), removal of carbonates (as well as sulfides, sulfates, oxides and hydroxides) by treatment with 6N HCl, removal of silicates by treatment with a mixture of 40% HF and 6N HCl. The acid treatments were done at 65-70°C while stirring with a PTFE coated magnetic stirrer. The solid residue was thoroughly washed with warm deionized water and water purified with a Direct-Q UV3 Millipore® System, and then dried at 40°C. Mineralogical analysis of the dried solid residues was conducted at the Institute of Earth

Sciences of the University of Lausanne using a Thermo Scientific ARL X-TRA Diffractometer, and confirmed the complete elimination of silicates (mainly clay minerals), which constituted up to 35% of the bulk rock samples before the HCl-HF treatment.

The stable isotope compositions are reported in the delta (δ) notation defined as

$$\delta^{i}\mathrm{E}_{sample/standard} = \frac{R\left({}^{i}\mathrm{E}/{}^{j}E\right)_{sample}}{R\left({}^{i}\mathrm{E}/{}^{j}\mathrm{E}\right)_{standard}} - 1$$

where R is the molar ratio of the heavy (^{i}E) to light (^{j}E) isotope of chemical element E (*e.g.*, $^{13}C/^{12}C$ or $^{15}N/^{14}N$). The standard for carbon isotope ratios ($\delta^{13}C$) is Vienna Pee Dee Belemnite limestone (VPDB), for nitrogen isotope ratios ($\delta^{15}N$) is molecular nitrogen in air (Air-N_2). For calibration and normalization of the measured isotopic ratios to the international scales, a 3- or 4-point calibration was used with international reference materials (RMs) and UNIL (University of Lausanne) in-house standards. The $\delta^{13}C$ and $\delta^{15}N$ values of the in-house standards were normalized with the RMs USGS64, USGS65 and USGS66. The RMs used together with the UNIL-standards for normalization and quality control of the measured $\delta^{13}C$ and $\delta^{15}N$ values were USGS-24, USGS-40, USGS-41 and IAEA-600. Average $\delta^{13}C$ value obtained for USGS-40 was –26.4 ± 0.1‰ (n = 6), which is in good agreement with accepted value of –26.39‰ (71). The accuracy of the analyses was checked periodically through the analysis of international reference materials. For $\delta^{15}N$, we obtained –4.5 ± 0.2‰ (n = 6) for USGS-40 and +1.0 ± 0.2‰ for IAEA-600, also in good agreement with accepted values of –4.52‰ and +1.0‰, respectively (71). The carbon and nitrogen concentrations (TOC and TN) were determined from the peak areas of the major isotopes using the calibrations for $\delta^{13}C$ and $\delta^{15}N$ values. The repeatability was better than 0.2 wt.% for carbon and nitrogen contents.

Additional nitrogen isotope analyses of bulk rock samples were carried out at the University of St. Andrews with an EA Isolink coupled via a Conflo IV to a MAT 253 IRMS (Thermo Fisher Scientific, Bremen, Germany). Untreated rock powders were weighed into tin capsules and combusted in a helium stream at 1020°C with a 5-sec pulse of O_2 gas (with a flow rate of 250 ml/min). Chromium oxide granules were used as an additional combustion aid in the reactor. SO_2 was trapped with silvered cobaltic cobaltous oxide in the reactor, while CO_2 and H_2O were trapped at room temperature with carbosorb and magnesium perchlorate, respectively. Nitrogen oxides were reduced to N_2 with a Cu column at 650°C, which also trapped excess of O_2 gas. N_2 was further purified with a GC column at 50°C. A blank was run

after each sample, and a set of standards was included before and after every set of five samples. USGS40 and USGS41 were used for isotopic calibration while SGR-1 was used as a quality control standard. We obtained a value of +17.4 ± 0.5‰ (n = 8) for SGR-1, which is in good agreement with previous measurements (+17.4 ± 0.4‰, ref. 72).

Acknowledgments: This study was funded by the University of Johannesburg, the National Research Foundation of South Africa (DST Innovation Research Fellowship to F. Ossa Ossa, Grant 75892 to A. Hofmann and the Centre of Excellence for Integrated Mineral and Energy Resource Analysis: CIMERA hosted by the University of Johannesburg) and the German Research Foundation DFG (Grant SCHO1071/7-1 to Ronny Schoenberg, University of Tübingen under the DFG-Priority Programme SPP-1833 "Building a Habitable Earth") and the University of Lausanne. AH thanks AngloGold Ashanti, Acclaim Exploration NL, J. Hancox and N. Hicks for access to drill core samples. JES thanks T. Adatte for XRD analysis. SWP acknowledges support from a Royal Society Wolfson Research Merit Award and a Leverhulme Research Fellowship. AB acknowledges support from the NSERC Discovery and Accelerator grants. We also thank the editor for careful handling our manuscript, and Kurt Konhauser and anonymous reviewer for their meaningful comments that significantly improved the manuscript.

References

1. Bekker A *et al*. (2004) Dating the rise of atmospheric oxygen. *Nature* 427: 117–120.
2. Farquhar J, Bao H, Thiemens M (2000) Atmospheric Influence of Earth's Earliest Sulfur Cycle. *Science*. 289 (5480): 756–758.
3. Kasting JF, Siefert JL (2002) Life and the Evolution of Earth's Atmosphere. *Science* 296 (5570): 1066–1068.
4. Anbar AD *et al*. (2007) A whiff of oxygen before the great oxidation event? *Science* 317 (5846): 1903–1906.
5. Garvin J, Buick R, Anbar AD, Arnold GL, Kaufman AJ (2009) Isotopic evidence for an aerobic nitrogen cycle in the latest Archean. *Science* 323 (5917): 1045–1048.
6. Wille M *et al*. (2007) Evidence for a gradual rise of oxygen between 2.6 and 2.5 Ga from Mo isotopes and Re-PGE signatures in shales. *Geochim. Cosmochim. Acta* 71 (10): 2417–2435.
7. Ossa Ossa F *et al*. (2018) Aerobic iron and manganese cycling in a redox-stratified Mesoarchean epicontinental sea. *Earth Planet. Sci. Lett* 500: 28–40.
8. Planavsky NJ *et al*. (2014) Evidence for oxygenic photosynthesis half a billion years before the Great Oxidation Event. *Nat. Geosci.* 7: 283–286.
9. Eickmann B, Hofmann A, Wille M, Bui TH, Wing BA, Schoenberg R (2018) Isotopic evidence for oxygenated Mesoarchaean shallow oceans. *Nat. Geosci.* 11: 133–138.

10. Albut G *et al*. (2018) Modern rather than Mesoarchaean oxidative weathering responsible for the heavy stable Cr isotopic signatures of the 2.95 Ga old Ijzermijn iron formation (South Africa). *Geochim. Cosmochim. Acta* 228: 157–189.

11. Satkoski A, Beukes NJ, Li W, Beard BL, Johnson CM (2015) A redox-stratified ocean 3.2 billion years ago. *Earth Planet. Sci. Lett.* 430: 43-53.

12. Homann M, Sansjofre P, Van Zuilen M, Heubeck C, Gong J, Killingsworth B, Foster IS, Airo A, Van Kranendonk MJ, Ader M, Lalonde SV (2018) Microbial life and biogeochemical cycling on land 3,220 million years ago. *Nat. Geosci.* 11: 665–671.

13. Lyons TW, Reinhard CT, Planavsky NJ (2014) The rise of oxygen in the Earth's early ocean and atmosphere. *Nature* 506: 307–315.

14. Kurzweil F, Wille M, Gantert N, Beukes NJ, Schoenberg R (2018) Manganese oxide shuttling in pre-GOE oceans – evidence from molybdenum and iron isotopes. *Earth Planet. Sci. Lett.* 452: 69–78.

15. Stüeken EE, Kipp MA, Koehler MC, Buick R (2016) The evolution of Earth's biogeochemical nitrogen cycle. *Earth-Sci. Rev.* 160: 220–239.

16. Stüeken EE, Buick R, Guy BM, Koehler MC (2015) Isotopic evidence for biological nitrogen fixation by molybdenum-nitrogenase from 3.2 Gyr. *Nature*: 520, doi:10.1038/nature14180.

17. Berman-Frank I, Lundgren P, Falkowski P (2003) Nitrogen fixation and photosynthetic oxygen evolution in cyanobacteria. *Res. Microbiol.* 154: 157–164.

18. Koehler MC, Buick R, Kipp MA, Stüeken EE, Zaloumis J (2018) Transient surface ocean oxygenation recorded in the ~2.66-Ga Jeerinah Formation, Australia. *Proc. Natl. Acad. Sci. U.S.A*, DOI: 10.1073/pnas.1720820115.

19. Falkowski PG (1997) Evolution of the nitrogen cycle and its influence on the biological sequestration of CO_2 in the ocean. *Nature* 387: 272–275.

20. Tyrrell T (1999) The relative influences of nitrogen and phosphorus on oceanic primary production. *Nature* 400: 525–531.

21. Reinhard CT *et al*. (2017) Evolution of the global phosphorus cycle. *Nature* 541: 386–389.

22. Poulton SW (2017) Early phosphorus redigested. *Nat. Geosci.* 10: 75–76.

23. Kipp MA, Stüeken EE (2017) Biomass recycling and Earth's early phosphorus cycle. *Sci. Adv.* 3 (11): DOI:10.1126/sciadv.aao4795.

24. Luo G *et al*. (2018) Nitrogen fixation sustained productivity in the wake of the Palaeoproterozoic Great Oxygenation Event. *Nat. Commun.* 9: DOI: 10.1038/s41467-018-03361-2.

25. Godfrey LV, Falkowski PG (2009) The cycling and redox state of nitrogen in the Archaean ocean. *Nat. Geosci.* 2: 735–729.

499 26. Cardona T, Sánchez-Baracaldo P, A. William Rutherford AW, Larkum AW (2018)
500 Early Archean origin of Photosystem II. *Geobiology*: DOI: 10.1111/gbi.12322.

501 27. Magnabosco C, Moore KR, Wolfe JM, &Fournier GP (2018). Dating phototropic
502 microbial lineages with reticulate gene histories. *Geobiology* 16: 179–189.

503 28. Shih PM, Hemp J, Ward LM, Matzke NJ, Fischer WW (2017). Crown group
504 Oxyphotobacteria postdate the rise of oxygen. *Geobiology* 15: 19–29.

505 29. Olson SL, Kump LR, Kasting JF (2013) Quantifying the areal extent and dissolved
506 oxygen concentrations of Archean oxygen oases. *Chem. Geol.* 362: 35–43.

507 30. Planavsky NJ, Rouxel OJ, Bekker A, Lalonde SV, Konhauser KO, Reinhard CT,
508 Lyons TW (2010) The evolution of the marine phosphate reservoir. *Nature* 467:
509 1088–1090.
510 31. Bjerrum CJ, Canfield DE (2002) Ocean productivity before about 1.9 Gyr ago limited
511 by phosphorus adsorption onto iron oxides. *Nature* 417: 159–162.

512 32. Konhauser KO, Lalonde SV, Amskold L, Holland HD (2007) Was there really an
513 Archean phosphate crisis? *Science* 315: 1234.

514 33. Wronkiewicz DJ, Condie KC (1989) Geochemistry and provenance of sediments
515 from the Pongola Supergroup, South Africa; evidence for a 3.0-Ga-old continental
516 craton. *Geochim. Cosmochim. Acta* 53 (7): 1537–1549.

517 34. Kappler A, Pasquero C, Konhauser KO, Newman DK, (2005) Deposition of banded
518 iron formations by anoxygenic phototrophic Fe(II)-oxidizing bacteria. *Geology* 33:
519 865–868.

520 35. Poulton SW, Canfield DE (2011) Ferruginous conditions: A dominant feature of the
521 ocean through Earth's history. *Elements* 7: 107–112.

522 36. Zhang K, Zhu X, Wood RA, Shi Y, Gao Z, Poulton SW (2018) Oxygenation of the
523 Mesoproterozoic ocean and the evolution of complex eukaryotes. *Nat. Geosci.* 11 (5):
524 pp. 345–350.

525 37. Ossa Ossa F *et al*. (2016) Unusual manganese enrichment in the Mesoarchean
526 Mozaan Group, Pongola Supergroup, South Africa. *Precambrian Res.* 281: 414–433.

527 38. Isson TT, Planavsky NJ (2018) Reverse weathering as a long-term stabilizer of
528 marine pH and planetary climate. *Nature*, DOI: 10.1038/s41586-018-0408-4.

529 39. Zegeye A et al. (2012) Green rust formation controls nutrient availability in a
530 ferruginous water column. Geology 40 (7): 599–602.

531 40. Halevy I et al. (2017) A key role for green rust in the Precambrian oceans and the
532 genesis of iron formations. Nat. Geosci. 10: 135–139.

533 41. Fogel ML, Cifuentes LA (1993) Isotope fractionation during primary production.
534 *Organic Geochemistry*, eds Engel MH, Macko SA (Plenum, New York), pp 73–98.

42. Stüeken EE, Buick R, Anderson RE, Baross JA, Planavsky NJ, Lyons TW (2017) Environmental niches and metabolic diversity in Neoarchean lakes. *Geobiology* 15(6):767–783.

43. Delarue F, Robert F, Sugitani K, Tartèse R, Duhamel R, Derenne S (2018) Nitrogen isotope signatures of microfossils suggest aerobic metabolism 3.0 Gyr ago. *Geochem. Perspect.* 7: 32–36.

44. Zhang X, Sigman DM, Morel FM, Kraepiel AM (2014). Nitrogen isotope fractionation by alternative nitrogenases and past ocean anoxia. *Proc. Natl Acad. Sci. USA* 111 (13): 4782–4787.

45. Lehman MR, Bernasconi SM, Barbieri A, McKenzie JA (2002) Preservation of organic matter and alteration of its carbon and nitrogen isotope composition during simulated and in situ early sedimentary diagenesis. *Geochim. Cosmochim. Acta* 66 (20): 3573–3584.

46. Ader M, Cartigny P, Boudou JP, Oh JH, Petit E, Javoy M (2006) Nitrogen isotopic evolution of carbonaceous matter during metamorphism: methodology and preliminary results. *Chem. Geol.* 232 (3–4): 152–169.

47. Ader M *et al*. (2016) Interpretation of the nitrogen isotopic composition of Precambrian sedimentary rocks: Assumptions and perspectives. *Chem. Geol.* 429: 93–110.

48. Lam P, Kuypers MM (2011) Microbial Nitrogen Cycling Processes in Oxygen Minimum Zones. *Annu. Rev. Mar. Sci.* 3: 317–345.

49. Anbar AD, Holland HD (1992) The photochemistry of manganese and the origin of banded iron formations. *Geochim. Cosmochim. Acta* 56 (7): 2595–2603.

50. Tebo BM, Johnson HA, McCarthy JK, Templeton AS (2005) Geomicrobiology of manganese(II) oxidation. *Trends Microbiol.* 13 (9): 421–428.

51. Clement BG, Luther III GW, Tebo BM (2009) Rapid, oxygen-dependent microbial Mn(II) oxidation kinetics at sub-micromolar oxygen concentrations in the Black Sea suboxic zone. Geochim. Cosmochim. Acta 73: 1878–1889.

52. Fuchsman CA, Murray JW, Konovalov SK (2008) Concentration and natural stable isotope profiles of nitrogen species in the Black Sea. *Mar. Chem* 111: 90–105.

53. Fulton JM, Arthur MA, Freeman KH (2012) Black Sea nitrogen cycling and the preservation of phytoplankton δ15N signals during the Holocene. *Glob. Biogeochem. Cycles* 26: doi:10.1029/2011GB004196.

54. Bekker A, Planavsky N, Krapež B, Rasmussen B, Hofmann A, Slack JF, Rouxel OJ, Konhauser KO (2014) Iron formations: Their origins and implications for ancient seawater chemistry. In: Holland, H.D., Turekian, K.K. (Eds.), Treatise of Geochemistry, second ed. Elsevier 9: 561–628.

55. Konhauser KO, Planavsky NJ, Hardisty DS, Robbins LJ, Warchola TJ, Haugaard R, Lalonde SV, Partin CA, Oonk PBH, Tsikos H, Lyons TW, Bekker A, Johnson CM

(2017) Iron formations: A global record of Neoarchaean to Palaeoproterozoic environmental history. Earth-Sci. Rev. 172: 140–177.

56. Busigny V, Lebeau O, Ader M, Krapež B, Bekker A (2013) Nitrogen cycle in the Late Archean ferruginous ocean. *Chem. Geol.* 362: 115–130.

57. Capone DG, Zehr JP, Paerl HW, Bergman B, Carpenter EJ (1997) Trichodesmium, a globally significant marine cyanobacterium. *Science* 276 (5316): 1221–1229.

58. Glass JB, Wolfe-Simon F, Elser JJ, Anbar AD (2010) Molybdenum–nitrogen colimitation in freshwater and coastal heterocystous cyanobacteria. *Limnol. Oceanogr*. 55 (2): 667–676.

59. Sverjensky DA, Lee N (2010) The great oxidation event and mineral diversification. *Elements* 6: 31–36.

60. Lalonde SV, Konhauser KO (2015) Benthic perspective on Earth's oldest evidence for oxygenic photosynthesis. *Proc. Natl. Acad. Sci. U.S.A* 112(4): 995–1000.

61. Wang X, *et al.* (2018) A Mesoarchean shift in uranium isotope systematics. *Geochim. Cosmochim. Acta* 238: 438–452.

62. Burron I, da Costa G, Sharpe R, Fayek M, Gauert C, Hofmann A (2018) 3.2 Ga detrital uraninite in the Witwatersrand Basin, South Africa: Evidence of a reducing Archean atmosphere. *Geology* 46(4): 295–298.

63. Koehler MC, Buick R, Barley ME (2018) Nitrogen isotope evidence for anoxic deep marine environments from the Mesoarchean Mosquito Creek Formation, Australia. *Precambrian Res.* 320: 281–290.

64. Babechuk MG, Widdowson M, Murphy M, Kamber BS (2015) A combined Y/Ho, high field strength element (HFSE) and Nd isotope perspective on basalt weathering, Deccan Traps, India. *Chem. Geol.* 396: 25–41.

65. Taylor S, McLennan S (1985) The Continental Crust: Its Evolution and Composition. *Blackwell*, London.

66. Poulton SW, Canfield DE (2005) Development of a sequential extraction procedure for iron: implications for iron partitioning in continentally derived particulates. *Chem. Geol.* 214 (3–4): 209–221.

67. Clarkson MO, Poulton SW, Guilbaud R, Wood RA (2014) Assessing the utility of Fe/Al and Fe-speciation to record water column redox conditions in carbonate-rich sediments. *Chem. Geol.* 382: 111–122.

68. Spangenberg JE, Jacomet S, Schibler J (2006) Chemical analyses of organic residues in archaeological pottery from Arbon Bleiche 3, Switzerland - evidence for dairying in the late Neolithic. *J. Archaeol. Sci.* 33 (1): 1–13.

69. Spangenberg JE, Bagnoud-Velásquez M, Boggiani PC, Gaucher C (2014) Redox variations and bioproductivity in the Ediacaran: evidence from inorganic and organic geochemistry of the Corumbá Group, Brazil. *Gondwana Res.* 26 (3–4): 1186–1207.

70. Durand B, Nicaise G (1980) Procedures for kerogen isolation. *Kerogen Insoluble Organic Matter from Sedimentary Rocks* eds Durand B (Editions Technip, Paris), pp 35–53.

71. Brand WA, Coplen TB, Vogl J, Rosner M, Prohaska T (2014) Assessment of international reference materials for isotope-ratio analysis (IUPAC Technical Report). *Pure Appl. Chem.* 86: 425–467.

72. Dennen KO, Johnson CA, Otter ML, Silva SR, Wandless GA (2006) delta 15N and non-carbonate delta 13C values for two petroleum source rock reference materials and a marine sediment reference material. *USGS,* 2006–1071.

Figures and Legends

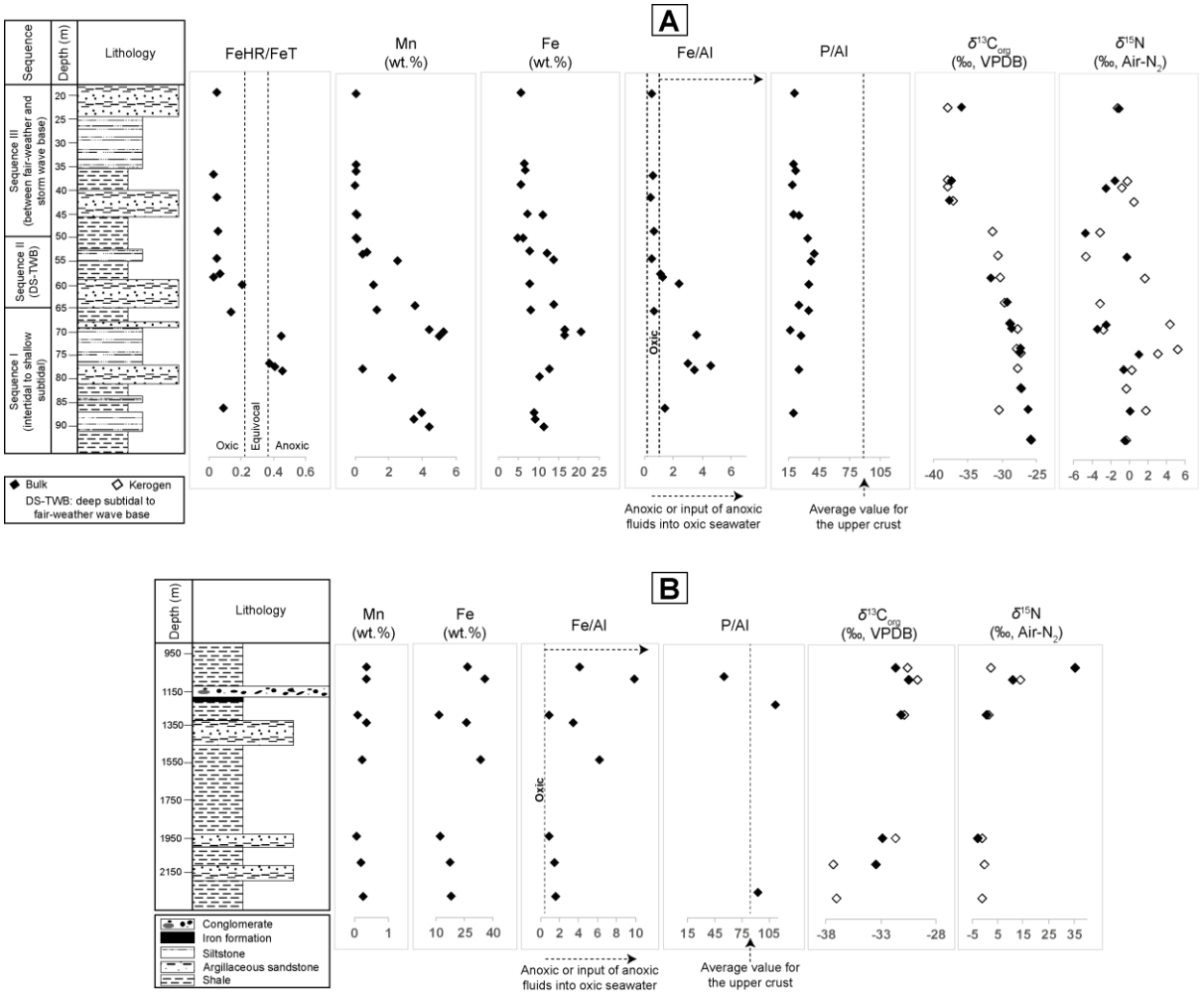

Fig. 1. Geochemical data for shale samples plotted along the lithostratigraphic columns of the studied sections of the Mozaan Group (**A**) from the shallow part of the Ntombe Formation in the White Mfolozi Inlier (Pongola basin), and (**B**) its deeper-water equivalent in the Nongoma area (see Fig. S2 for details). Sequences are defined based on water depth indicators and chemostratigraphic data. Vertical lines and horizontal arrows on Fe/Al plots are based on the description provided in analytical methods (ref. 67), whereas the average value for the upper crust on P/Al plots is from ref. 65.

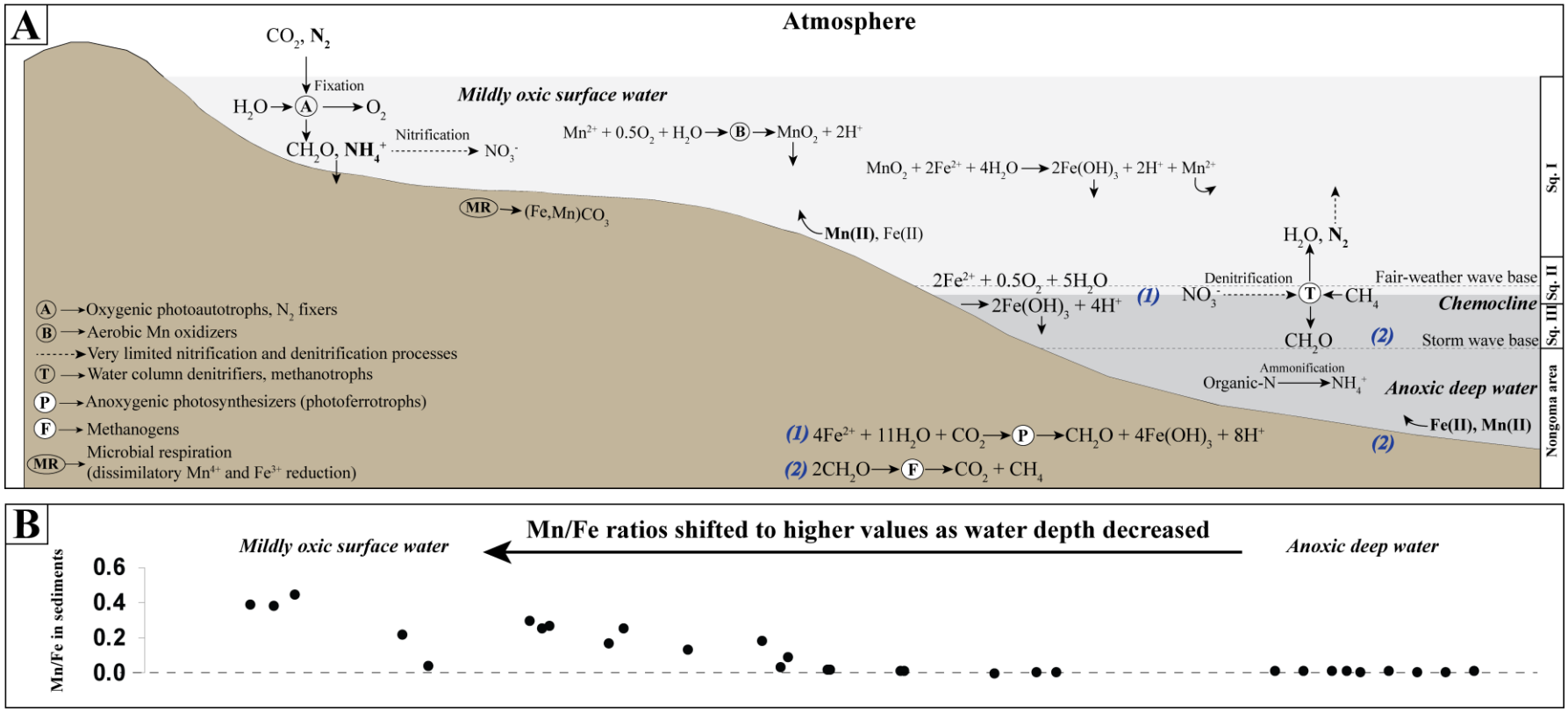

Fig. 2. Proposed paleoenvironmental reconstruction of the Mesoarchean Pongola basin during deposition of the Ntombe Formation, Mozaan Group (modified from ref. 7). **(A)** Water column chemistry and biogeochemical cycles developed in the localized oxygenated surface waters (recorded by the sequences I and II), overlying anoxic deep-waters (recorded by the sequence III and the sedimentary succession in the Nongoma area). Low biological O_2 production in shallow-marine environments likely limited expression of nitrification and denitrification signals in sediments deposited in the Pongola basin **(B)** Mn/Fe ratios in sediments reflective of seawater redox increase towards the shoreline as ferruginous waters upwelled from anoxic, deep settings to mildly oxygenated, shallow-marine environments. Sq. I (sequence I); Sq. II (sequence II); Sq. III (sequence III).

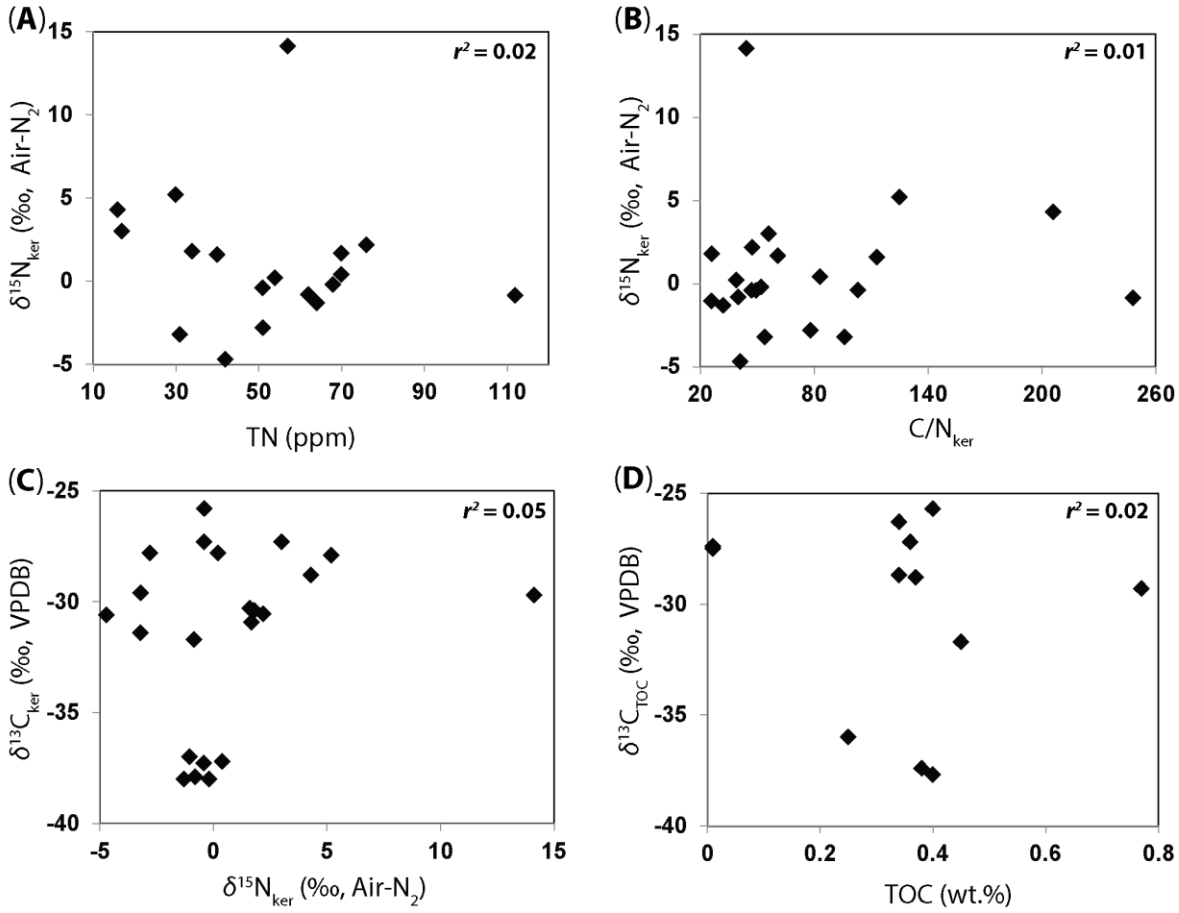

641

642

643 **Fig. 3.** Cross-plots showing relationships among C and N elemental and isotopic data, with
644 no obvious co-variation among these parameters suggesting a minimal impact of post-
645 depositional processes on the original C and N isotopic composition of the marine biomass.
646 (**A**) TN *vs*. $\delta^{15}N$ of kerogen ($\delta^{15}N_{ker}$); (**B**) Atomic C/N ratios in kerogen (C/N_{ker}) *vs*. $\delta^{15}N_{ker}$;
647 (**C**) $\delta^{15}N_{ker}$ *vs*. $\delta^{13}C_{org}$ of kerogen; (**D**) TOC *vs*. $\delta^{13}C_{org}$ of bulk sediment.